Broadband all dielectric high refractive index metamaterials in the terahertz region

YANYAN DONG[1,2], CHENXIA LI[2], XUFENG JING[2], JIANPING HU[1,*]
[1]*The Faculty of Information Science and Technology, Ningbo University, Ningbo, 315211, China*
[2]*Institute of Optoelectronic Technology, China Jiliang University, Hangzhou 310018, China*

We design an all-dielectric broadband terahertz-band high-refractive metamaterial sensor. The structure is composed of a single-layer square column structure based on ultra-high dielectric constant materials, and exhibits a square periodic arrangement. The S-parameter inversion algorithm calculates that the effective refractive index is above 15 in the 2.48THz ~ 2.97THz band, and the peak value is above 16. At the same time, we reveal the effects of cell size, cell height, period, etc. on the effective permittivity, permeability, impedance, refractive index, and frequency bandwidth of the structure and their changing trends. We further propose a metamaterial structure with four square pillars of different sizes within the unit structure. The effects of square pillar size, square pillar height and cell base height on the effective refractive index of the metamaterial structure were studied respectively. This square-pillar composite structure metamaterial has more degrees of freedom, and can control the effective refractive index of the metamaterial, and the peak refractive index can reach more than 18.

1. Introduction

Metamaterials are artificially designed, composite structures that do not exist in nature [1-8]. D. Smith's rational combination of metal wire and metal split resonator is the first to realize a metamaterial substance with negative permittivity and magnetic permeability at the same time [9]. In addition to negative-index metamaterials, researchers are also investigating high- and zero-index properties in the refractive index spectrum. With the advent of metamaterials, controlling the electromagnetic properties of metamaterials has gone beyond the limits achievable with naturally occurring matter [10-20]. Extending the refractive index of metamaterials into the high normal range will refine the achievable refractive index spectrum and could provide greater design flexibility for transformation optics [21, 22]. Except for a few insulators and semiconductors with high refractive index in certain or some special wavelength bands, the refractive index of existing materials in nature is also limited, and the highest refractive index of materials is about 3.0 [23]. A few semiconductors and insulators, such as lead, sulfide, or strontium titanate, exhibit fairly high peak refractive indices at mid- and far-infrared frequencies [23]. In addition to the above materials, there are very few naturally occurring transparent materials with a high positive refractive index.

Recently, experiments have demonstrated that large-area, free-standing, flexible terahertz metamaterials composed of strongly coupled unit cells can achieve broadband high-refractive-index properties [23]. Thus, expanding the high refractive index will launch the scope of spectral research of refrative index material. Previous work on improving the refractive index of the metamaterial by designing metamaterials frequently in atoms [24], or split-ring resonator [25]. In order to obtain high refractive index metamaterials, Sievenpiper *et al.* [26] proposed that a parallel plate capacitor with subwavelength array could enhance the effective permittivity. But, the effective permeability was simultaneously reduced due to the diamagnetic effect, leading to slightly enhancement of the effective refractive index. Interestingly, Wood *et al.* [27] proposed a close packed array of metallic cubes, which revealed the diamagnetic effect was attributed to the induced current loops in cubes. Shin *et al.* [28] demonstrated that the diamagnetic effect can be decreased by reducing the volume enclosed by the induced surface currents through structured cubes. By using appropriate structured cube elements, a larger improvement of the effective refractive index of metamaterial can be obtained with increasing the effective permittivity by the capacitive coupling effect and increasing the effective permeability by decreasing the diamagnetic effect. Previous work to achieve high refractive index properties mainly exploited the strong coupling effect of metallic structures [26-28]. Metal materials are easy to oxidize and

corrode. Especially in high-power and high-temperature applications, the disadvantages of metal metamaterials are more obvious [29-42]. Therefore, it is necessary to further study all-dielectric type high refractive index metamaterials.

Although Li et al. reported all-medium high refractive index metamaterials [43], such metamaterials are only effective in a narrow band range. In this paper, a broadband high-refractive-index metamaterial sensing device in the terahertz band is designed by using high-dielectric-constant ceramic materials. Our calculations found that the designed metamaterial structures have ultra-high refractive index values, which are unattainable for naturally occurring materials. We further study the influence of the square pillar structure size, square pillar height, substrate thickness, substrate height and other factors on the refractive index of metamaterials. The unnaturally high refractive index metamaterials with various artificial atoms will fill up the spectrum of attainable refractive index, and they will provide more flexibility in device design, such as, metamaterial cloaking in transformation optics and slow light devices. Also, the high refractive index metamaterials have important applications in high resolution imaging and lithography, where the resolution is proportional to the refractive index.

2. The principle of high refractive index of metamaterials

The effective refractive index of a material can be expressed as $n = \sqrt{\varepsilon_r \mu_r}$, and we can increase the refractive index by studying ε_r and μ_r. A parallel line charge accumulation model can be applied to estimate the effective refractive index of metamaterials [23]. The accumulated charges and the scaling of the effective permittivity depended on the gap width between elements. In strongly coupled reigme, the accumulated charges were proportional to $L^3 g^{-1}$, and they can be represented as [23]

$$Q \propto \varepsilon_0 \varepsilon_p \frac{L^3}{g} E_{in} , \quad (1)$$

where ε_p is the relative permittivity of the substrate material, L is the length of the unit cell of metamaterial, g is the gap width between metal elements, and E_{in} is the incident electric field. The effective permittivity of the metamaterial can be estimated by

$$\varepsilon_r = \varepsilon_p + \frac{P}{\varepsilon_0 E} , \quad (2)$$

where P is the polarization density, $E = (L/g)^\beta E_{in}$, and it can be approximated by dipole moment per unit volume as

$$P = \frac{Q(L-g)}{L^2 d} \quad (3)$$

Here, d is the physical thickness of the unit cell of the metamaterial. The effective refractive index can be expressed as

$$n \cong n_p \alpha^{1/2} d^{-1/2} L^{(2-\beta)/2} g^{-(1-\beta)/2} \quad (4)$$

where α and β are dimensionless fitting parameters.

3. High-refractive-index metamaterials

Based on the basic theory of high refractive index, the effective permittivity and effective permeability of the material affect its refractive index. We designed a structure in which square columns made of ceramic material are arranged periodically, and a layer of PI flexible material substrate of the same square column is placed on the bottom and top of the structure, as shown in Fig. 1. The real part of the dielectric constant of the ceramic material is 72 and the imaginary part is 0.18. In this structure, the side length of the ceramic square column is f, the height is t, the side length of the base is e, and the base thickness is l. The period of the structure in both the X and Y directions is e. After optimization, the height of the square column is t = 10 μm, and the side length f = 14 μm. The thickness of the structural substrate is l = 5 μm, and the side length e = 42 μm. The refractive index of ceramic materials is 72, but the refractive index of natural materials is basically constant. By designing the metamaterial structure, the equivalent refractive index can be adjusted freely according to the change of structure size.
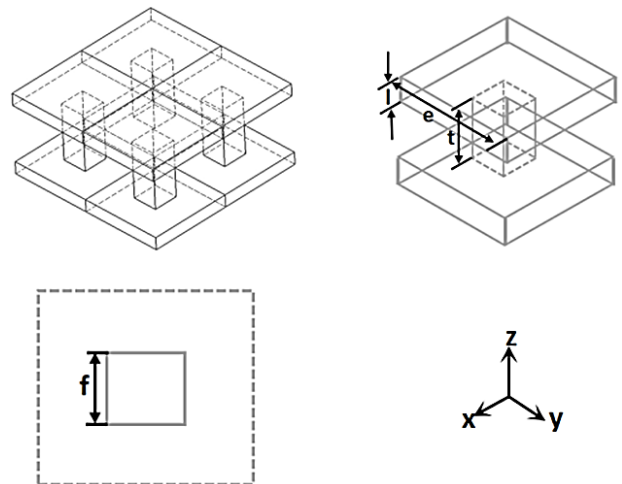
Fig. 1. Single square column metamaterial structure

When the incident light is incident along the Z axis, the high dielectric constant ceramic particles can act as a dielectric to treat the resonator. Due to the open circuit state at the medium-air interface, the electromagnetic waves are reflected to the inner walls of the dielectric particles and the power inside the medium is limited, which leads to different resonance modes within the dielectric resonant cavity. Due to the high permittivity of ceramic particles, the medium-air interface can be regarded as a perfect magnetic conductor, where the tangential component of the magnetic field or the normal component of the electric field disappears. The rectangular dielectric resonator is analyzed by the hybrid magnetic wall method. The surface of the high dielectric constant ceramic can be regarded as a magnetic wall. When electromagnetic waves enter the ceramic, they are reflected at the medium-air interface, forming standing waves and resonating. Dielectric resonators excite magnetic or electrical resonances, resulting in resonances of effective permittivity or permeability. In order to obtain a broadband high refractive index effect, the structure provided in this study is designed according to two considerations of increasing the dielectric constant and reducing the diamagnetic effect.

Fig. 2 shows the S-parameters and corresponding phases of the metamaterial structure. As shown in Fig. 3, based on the S-parameter extraction algorithm [44-47], we extracted the effective permittivity, effective permeability, effective impedance, and effective refractive index of the metamaterial structure. S11 represents the reflection coefficient and S21 represents the transmission coefficient. It can be seen from Fig. 3(a) and Fig. 3(b) that both the effective permittivity and effective permeability appear strong resonance. When the frequency increases to around 3.02THz, the dielectric constant first reaches the maximum value and then drops to the minimum value, as shown in Fig. 3(a). And this characteristic of the effective permeability curve always occurs at the electrical resonance, as shown in Fig. 3(b). We used finite integral methods to calculate the S-parameters and the electromagnetic field distribution. Effective permeability and effective permittivity have similar characteristics. Due to the effect of magnetic resonance, as the frequency increases, the effective permeability also first reaches a maximum value and then decreases to a minimum value.

Within the calculated frequency range, Mie resonance phenomena, including magnetic dipole resonance, electric dipole resonance and magnetic quadrupole resonance, occur within the metamaterial. Mie resonance is a resonance scattering phenomenon based on Mie scattering theory. In electromagnetics, Mie theory assumes that the scattered light of large particles is due to the superposition of light radiation caused by the dipole, quadrupole, octupole and higher electron multipole oscillators of electrons in the particle, which is the solution of electromagnetic radiation to spherical particles of arbitrary size obtained by Maxwell equation. If the scattering is not rigid and has strong resonance properties, then the scattering will be affected by resonance, resulting in Mie resonance.

In Fig. 3(a), at the frequency where the two effective dielectric constants have peaks, in Fig. 3(b) the effective permeability is a relative trough at this frequency. The signs of $d\mu/d\lambda$ and $d\varepsilon/d\lambda$ are opposite, while the permeability at the peak of the dielectric constant is close to 0. The impedance shown in Fig. 3(c) can explain why the stop band is formed. When magnetic resonance occurs, impedance matching becomes poor, resulting in reduced transmission. At around 2.45 THz, the effective permeability reaches a negative maximum, while the effective permittivity is positive, which results in a polar impedance mismatch at 2.45THz, resulting in the first transmission attenuation in Fig. 2(a). At around 3.04 THz, the effective permittivity reaches a negative maximum, while the effective permeability returns to positive, which correspondingly leads to the second transmission decay in Fig. 2(a). Between the two resonances, the impedance approaches zero, forming a stop band. As shown in Fig. 3(d), a wide band is formed between 2.45 THz and 3.04 THz, however, its refractive index peak is around 4.0, and the average refractive index of the entire broadband is around 3.0. In numerical simulation, the finite integral method was used to calculate the transmission and reflection coefficients of cell structures. In the simulation of unit structure, unit cell boundary and open boundary were applied. We used the finite integral method to calculate the near-field distribution characteristics of metamaterials. The equivalent parameters of metamaterials were extracted using S parameter inversion algorithm.
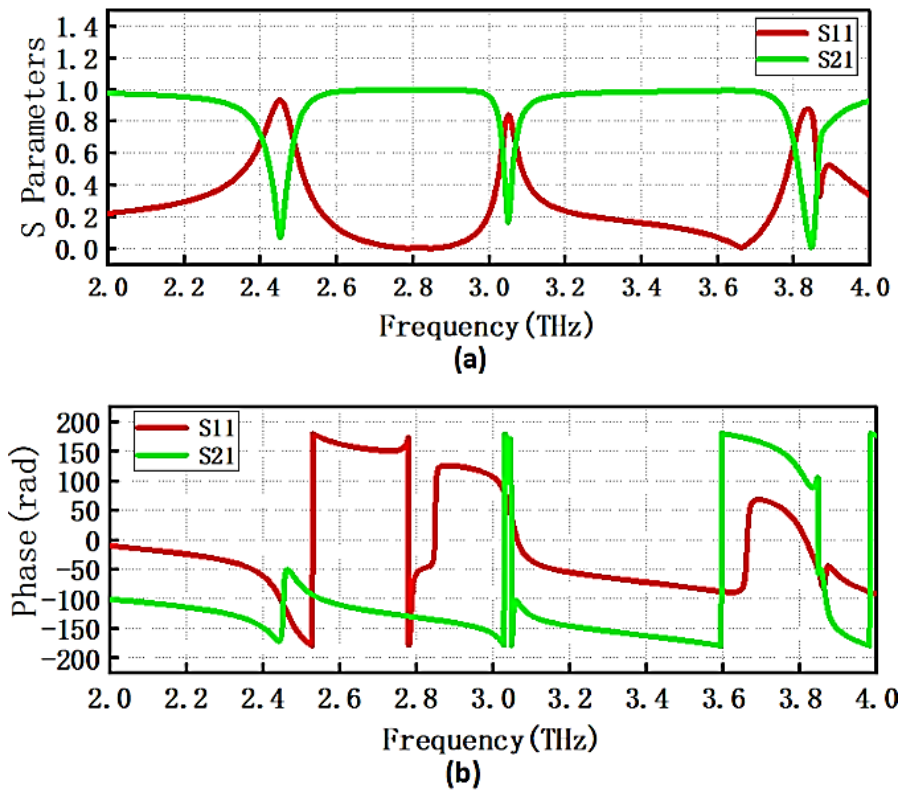
Fig. 2. (a) S11, S21 amplitude, (b) S11, S21 phase (color online)
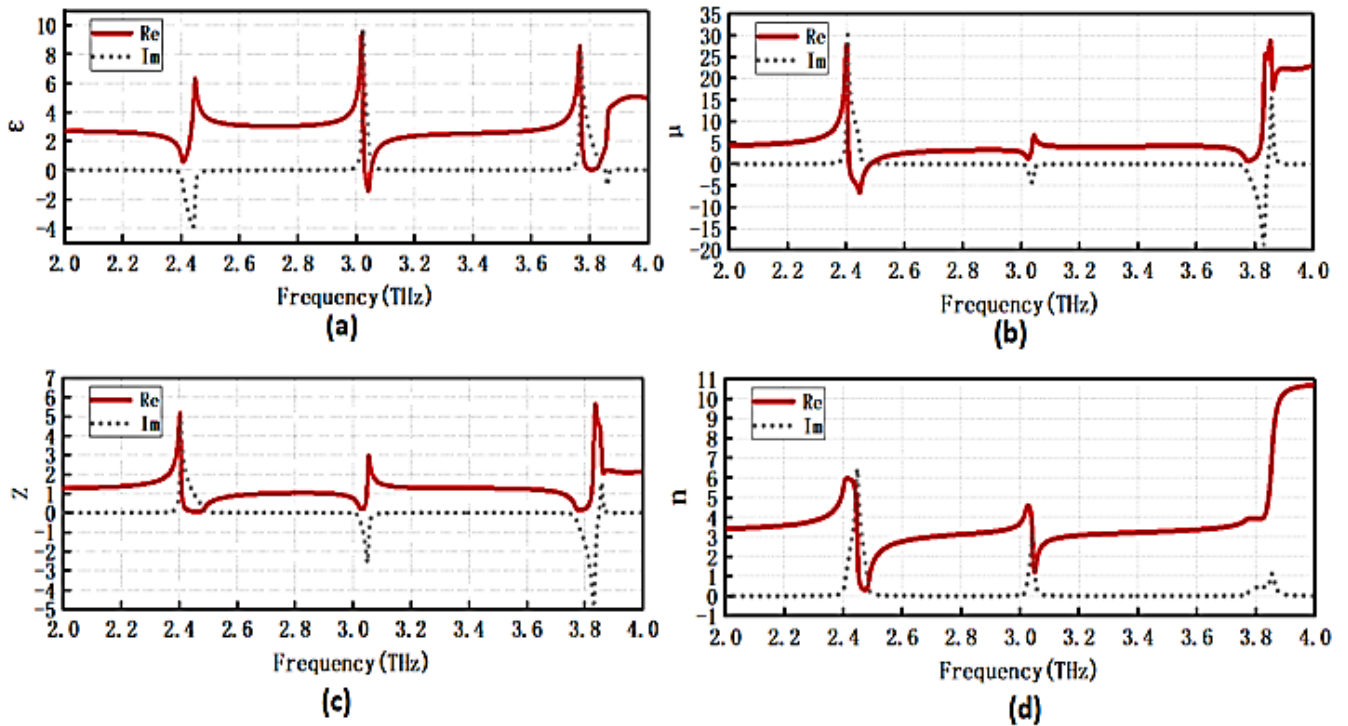
Fig. 3. (a) Effective permittivity, (b) effective permeability, (c) impedance, (d) refractive index (color online)
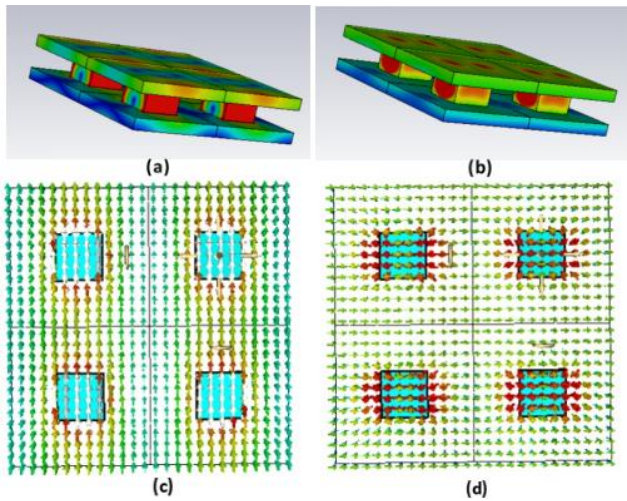
Fig. 4. (a) Spatial distribution of electric field in a single square column periodic structure (b) Spatial distribution of magnetic field in a single square column periodic structure (c) Spatial distribution of electric field in a single square column periodic structure (d) Spatial distribution of magnetic field in a single square column periodic structure (color online)

The electromagnetic field distribution of a single square column is shown in Fig. 4. Fig. 4 depicts the electromagnetic field (2.42 THz) on the surface of a single square column structure when the incident light is perpendicular to the single square column structure along the Z direction. As shown in Fig. 4(c), the incident electric field accumulates a large amount of charges at the edge of each square column, especially at the long edge of the square column along the x-direction. A huge dipole moment is generated at the edge along the x-direction, the electric field strength in the gathering direction is larger than the incident electric field strength, and the effective dielectric constant of a single square column is greatly improved. Suppressing the diamagnetic effect of the single square column structure is another way to improve the effective refractive index of the designed single square column structure. Fig. 4(b) shows the magnetic field distribution, the effective permeability has both real and imaginary parts, and the structure has a diamagnetic effect.

To improve the bandwidth of high-refractive-index metamaterials, we propose a novel single-unit cell structure, as shown in Fig. 5. On the basis of a single square column, a composite structure of four square columns with different side lengths is proposed, and other conditions remain unchanged. It can be seen from Fig. 5 that the side lengths of the four ceramic square columns in the structure are a, b, c, and d, respectively. The height is t', the base side length is e', and the thickness is l'. The period of the structure in both the X and Y directions is e'. In the initial structure, the height of the four square columns is t'

= 10 μm, and the side lengths are a = 7 μm, b = 10.5 μm, c = 14 μm, and d = 17.5 μm, respectively. The substrate thickness is l' = 5 μm, and the side length is e' = 42 μm. The structure is simulated under the same environment. Since the incident light is incident vertically along the z-axis, and the side lengths of the square-column composite structure are different, two modes are calculated. The incident light is incident polarized along the y-axis (called the TE mode), and the incident light is incident polarized along the x-axis (called the TM mode). The structural parameters are extracted through the S-parameter inversion algorithm, and the structural equivalent parameters are shown in Fig. 6.

We design a superunit structure in which the superunit consists of four different all-dielectric particles. Mie resonance is a kind of structural resonance at electromagnetic frequency. When the size of the particle is close to the wavelength of electromagnetic wave, the interaction between electromagnetic wave and particle will occur. When the particles are close to each other, electromagnetic wave will be concentrated in the near field condition. When the density of the electromagnetic field is high enough, it ionizes the medium. We can think that the resonance of electromagnetic wave has a linear relationship with the structure size. Particles of different sizes cause resonance at different frequencies. So, we design four particles of different sizes in a supracellular, and expect to achieve resonance at different frequencies. Moreover, the four particle sizes are not too far apart, so the four resonant frequencies overlap and cross, resulting in wide-band resonance characteristics.
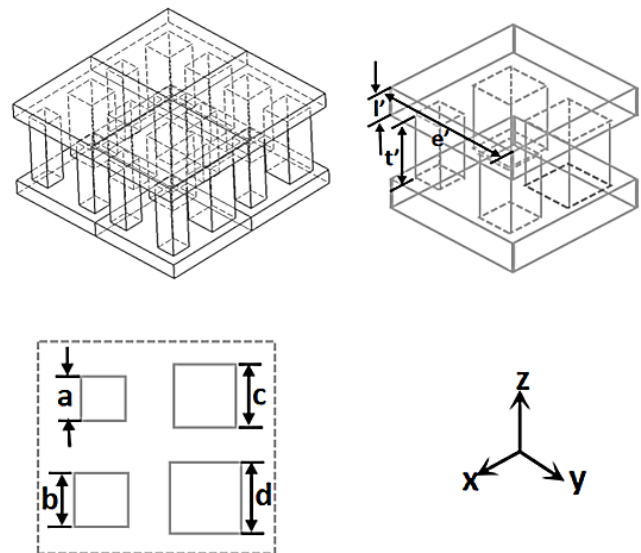
Fig. 5. Metamaterial structure composed of square columns
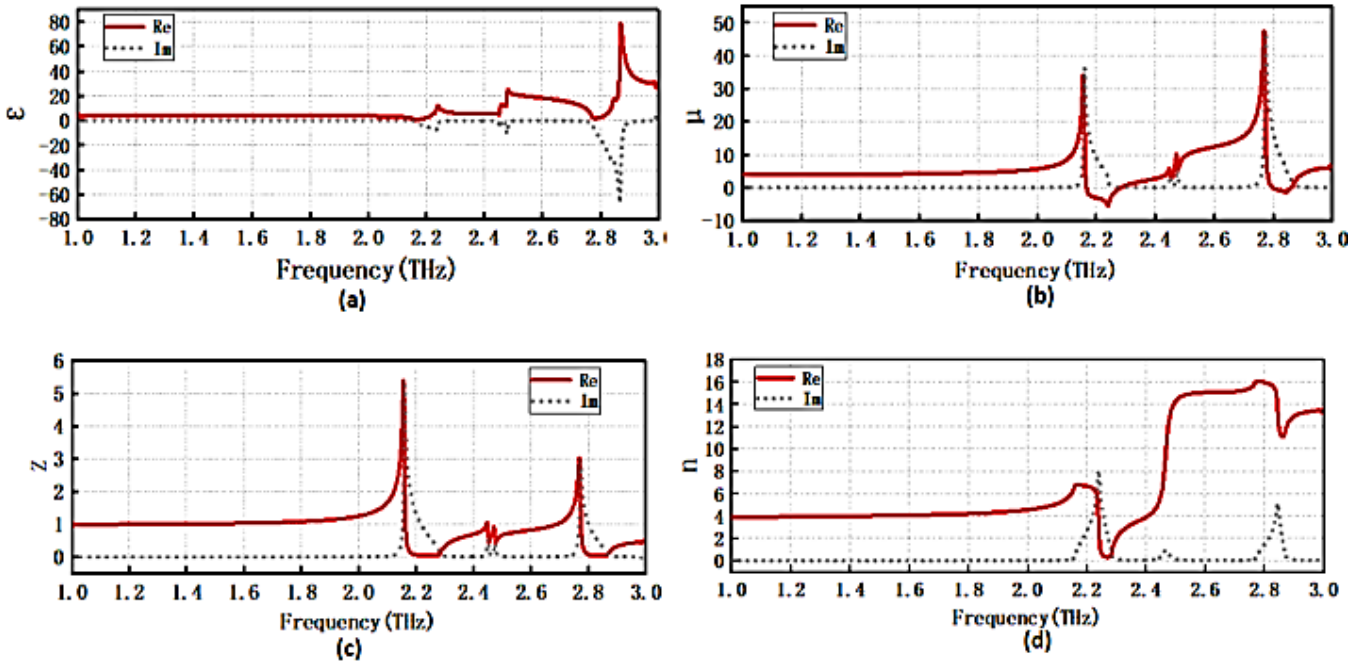
Fig. 6. (a) Effective permittivity, (b) effective permeability, (c) effective impedance, (d) effective refractive index

As shown in Fig. 6, based on the S-parameter inversion algorithm, we extracted the effective permittivity, effective permeability, effective impedance and effective refractive index of the metamaterial structure. It can be seen from Fig. 6(a) and Fig. 6(b) that both the effective permittivity and effective permeability appear strong resonance. As shown in Fig. 6(a), when the frequency is increased to around 2.97 THz, the dielectric constant reaches a maximum value. This characteristic of the effective permeability curve always occurs at electrical resonance. As shown in Fig. 6(b), due to the effect of magnetic resonance, with the increase of frequency, the effective permeability first reaches the maximum value and then decreases. The effective impedance shown in Fig. 6(c) can explain the generation of the stop band. When magnetic resonance occurs, impedance matching becomes poor, resulting in reduced transmission. Thus, two transmission attenuations are generated in the corresponding frequency range. And between the two resonances, the impedance is close to zero, forming a stop band. As shown in Fig. 6(d), a bandwidth is formed between 2.48 THz and 2.97 THz, the peak of the refractive index is about 16, and the average refractive index of the whole broadband is about 15. This is impossible for most materials that exist in nature. This metamaterial structure design meets our expected design results.

The electromagnetic field of the combined structure of four square columns is shown in Fig. 7. The electromagnetic field (2.40 THz) on the surface of the combined structure of the square column is described when the incident light is perpendicular to the structure along the Z direction. As shown in Fig. 7(c), the incident electric field accumulates a large amount of charges at the

edge of each square column, especially at the edge of the long side of the square column along the y-direction.
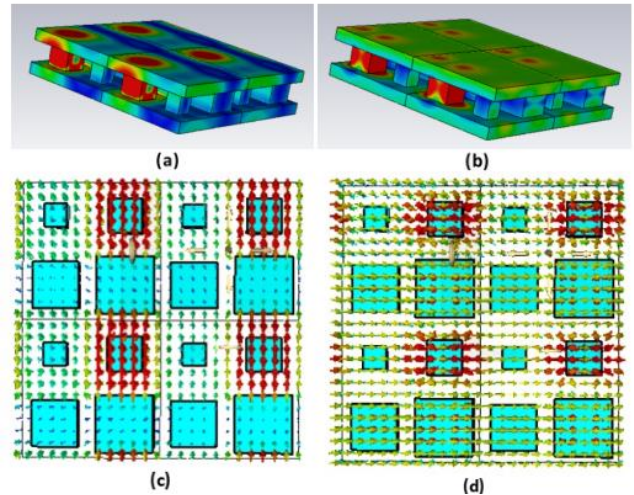
Fig. 7. (a) Spatial distribution of the electric field in the periodic structure of the composite square column (b) Spatial distribution of the magnetic field in the periodic structure of the composite square column (c) Spatial distribution of the electric field in the periodic structure of the composite square column (d) Spatial distribution of the magnetic field in the periodic structure of the composite square column (color online)

The large amount of accumulated charges produces a huge dipole moment at the edges of the square pillars that are close to each other along the y-direction. The electric field strength is large, and the effective dielectric constant of the four square column groups is greatly improved.

Suppressing the diamagnetic effect of the four-square-pillar combined structure is another method to improve the effective refractive index of the designed square-pillar structure. Fig. 7(b) shows the magnetic field distribution, the effective permeability has both real and imaginary parts, and the structure has a diamagnetic effect.

Next, we can study the effect of structural parameter changes on the effective permittivity, effective permeability, impedance, and refractive index of the metamaterial. First, the effect of the side length of the square cylinder on the refractive index is demonstrated. When studying the influence of the side length of the square column on the refractive index, the side length is proportionally enlarged by 1.1 times and 1.2 times. The

height of the square column is always 10 μm, the side length and thickness of the base are unchanged, and the period is always 42 μm. We only analyze the real part change of each effective parameter. We assume that the initial single square column structure is R1, the side length is proportionally expanded by 1.1 times as R2, and the side length is proportionally expanded by 1.2 times as R3. Then we can make corresponding changes to the periodic structure of the four square pillars. Let the initial structure be R1', the side length proportionally enlarged by 1.1 times is set as R2', and the side length is proportionally enlarged by 1.2 times as R3'. Observe the changing trend of each parameter. The parametric curves are compared in Figs. 8, 9, and 10.
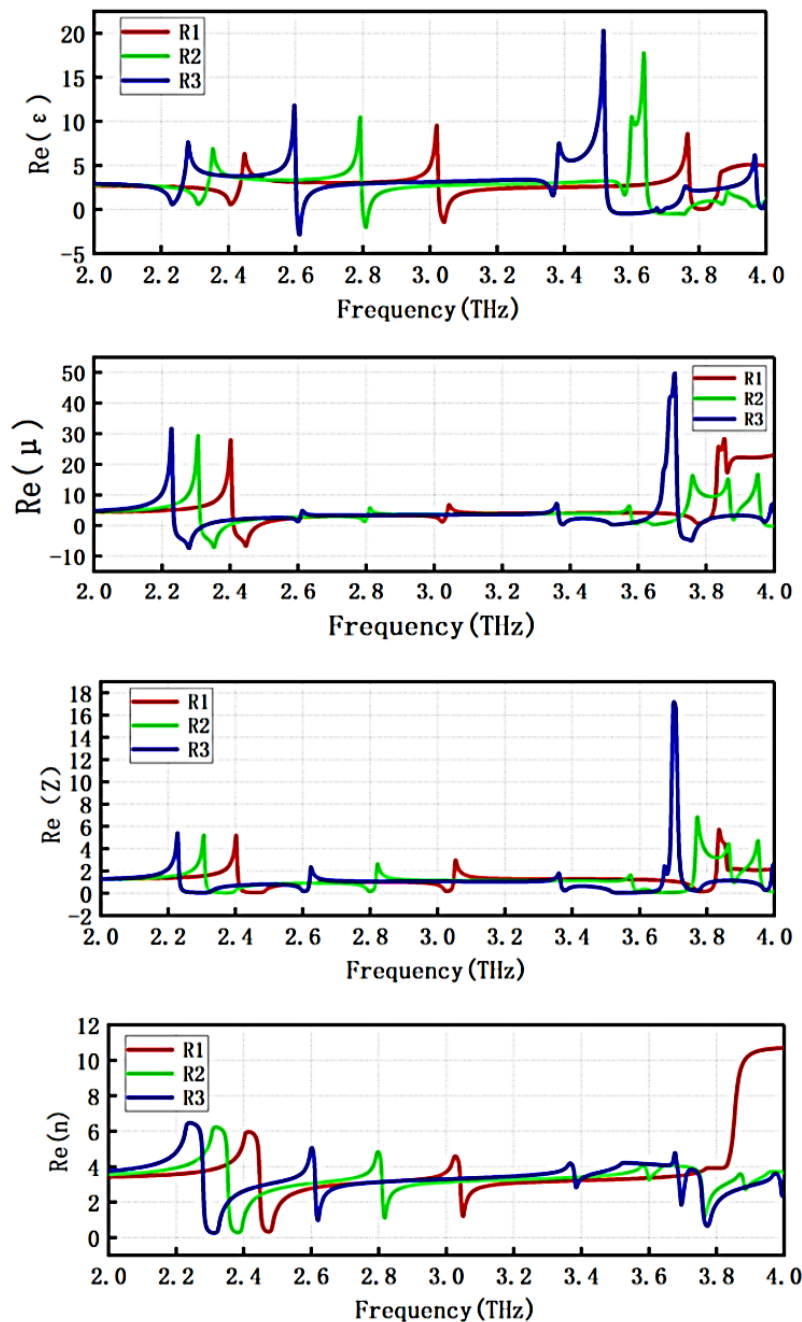
Fig. 8. The side length of a single square column changes proportionally (color online)
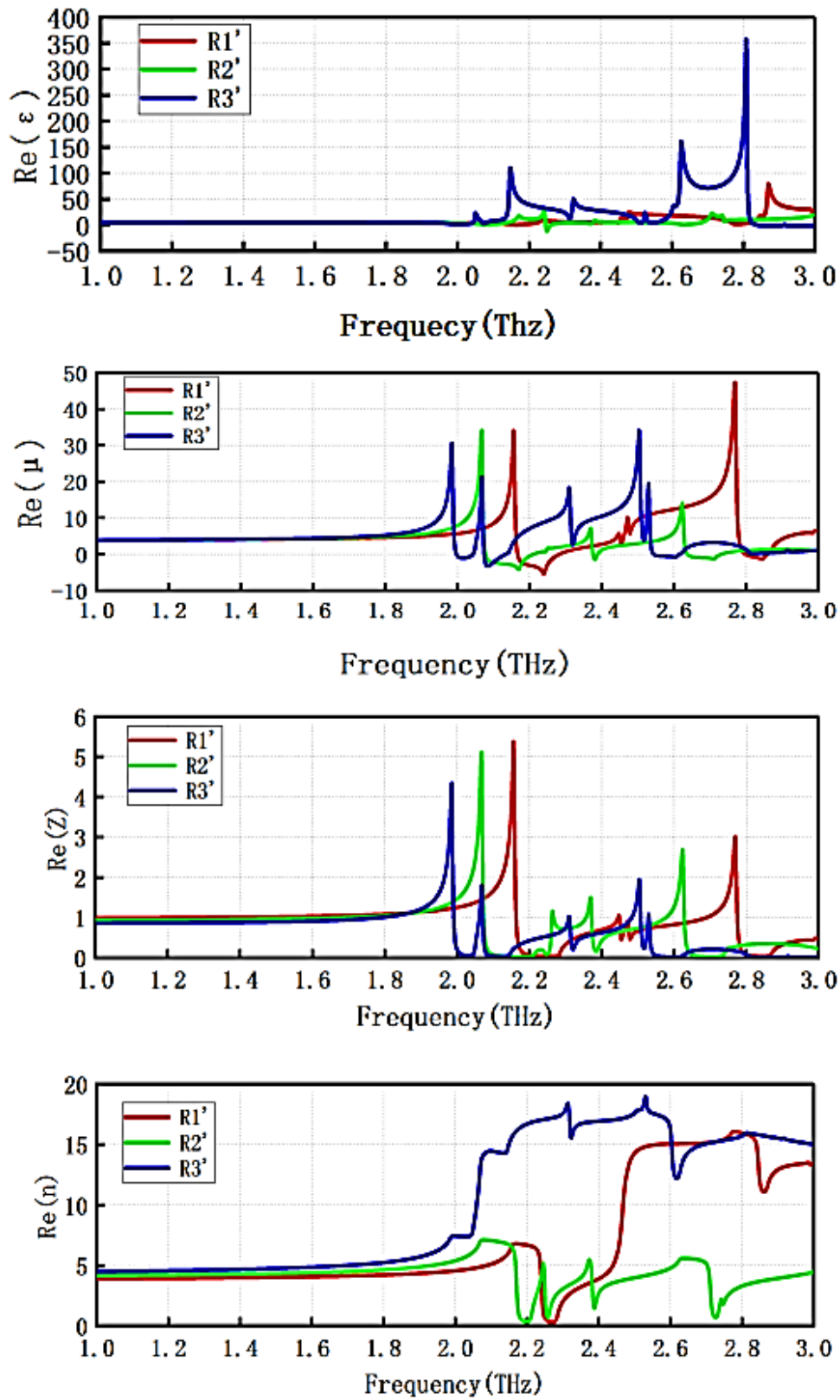
Fig. 9. Equal-proportion change of side length of square-column composite structure incident in TE mode (color online)
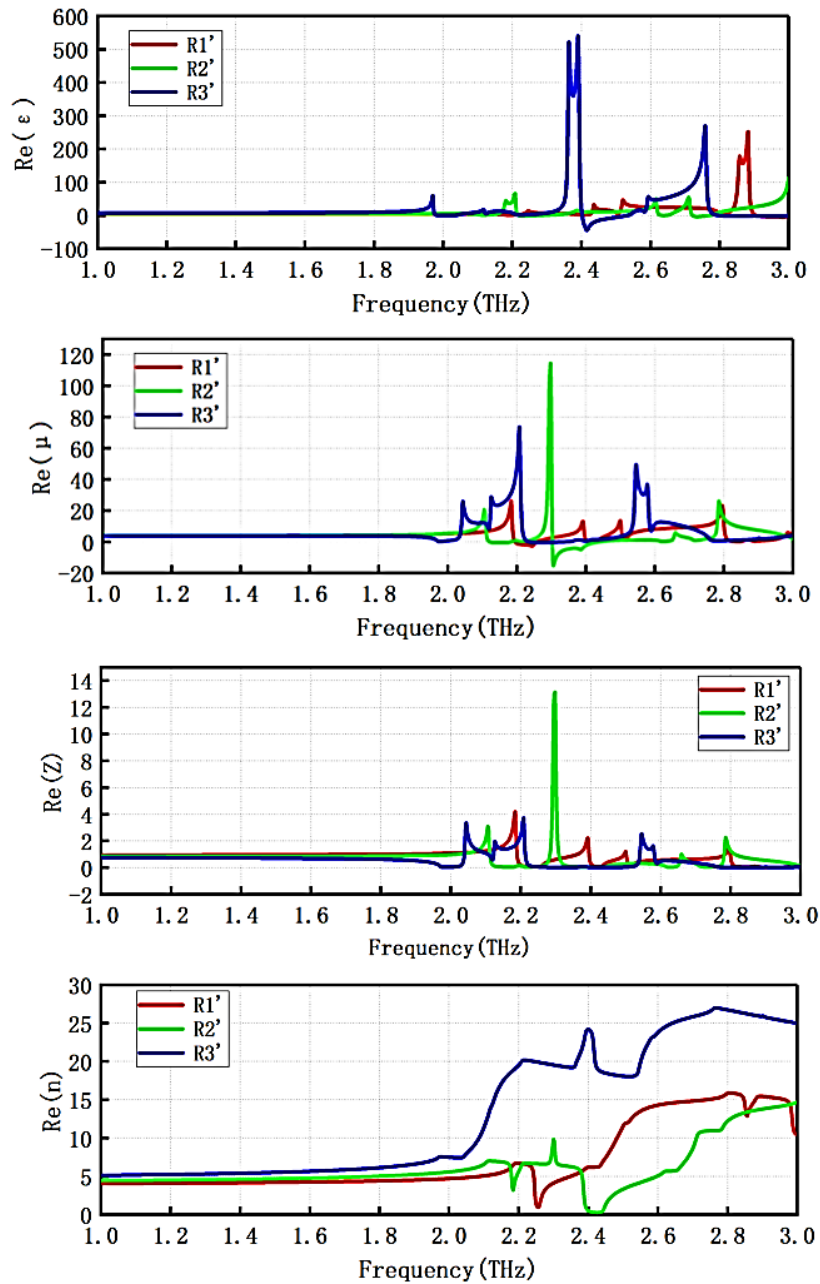
Fig. 10. Equal-proportion change of side length of square-column composite structure incident in TM mode (color online)

As shown in Fig. 8, with the increase of the side length of a single square column structure, the resonance peak value of the effective dielectric constant becomes larger, and the frequency value corresponding to the peak value becomes smaller and smaller. The changing trends of effective permeability and effective impedance are the same as those of effective permittivity. The effective refractive index peak has an increasing trend, but the change is not very obvious. As the peak becomes larger, the frequency corresponding to the peak becomes smaller and smaller. As shown in Fig. 9, when the TE mode is incident, the lengths of each side of the combination of four square columns are proportionally enlarged by 1.1 times and 1.2 times. Compared with R1' and R3', the effective dielectric constant curve R2' has no obvious peak, and the whole curve tends to a straight line with very little change. The effective permeability of R2' is smaller than that of R1' and R3', and the effective permeability of R3' is smaller than that of R1'. The frequency corresponding to the peak becomes smaller and smaller as the side length increases. The effective refractive index of R2' has no obvious broadband, but R3' has obvious broadband, and the frequency corresponding to the peak of the broadband refractive index is smaller than that of R1', the interval corresponding to the bandwidth is greater than that of R1', and the peak value is about 19THz. As shown in Fig. 10, in the case of TM mode incident, the parameter change curve is similar to the TE change. To sum up, when the

side length of the square-column composite structure is expanded to 1.2 times, the side lengths are a=8.4 μm, b = 12.6 μm, c = 16.8 μm, d = 21 μm, and the effective parameters of the metamaterial structure are ideal.

Next, we investigate the effect of the square column height on the refractive index. When studying the influence of the height of the square column on the refractive index, according to the optimization of the composite structure of the square column, the side lengths are a = 8.4 μm, b = 12.6 μm, c = 16.8 μm, and d = 21 μm, respectively. The structure heights are reduced to 9 μm and

8 μm, respectively. The substrate side length and thickness are unchanged, and the period is always 42 μm. We select a single square column to expand the side length by 1.2 times, that is, f = 16.8 μm, and other conditions remain unchanged. The height variation of a single square pillar structure is t = 10 μm, t = 9 μm and t = 8 μm. The height variation of the composite periodic structure of the four square pillars is t' = 10 μm, t'=9μm and t' = 8 μm. The effective parameter changes of metamaterials are shown in Figs. 11, 12 and 13, respectively.
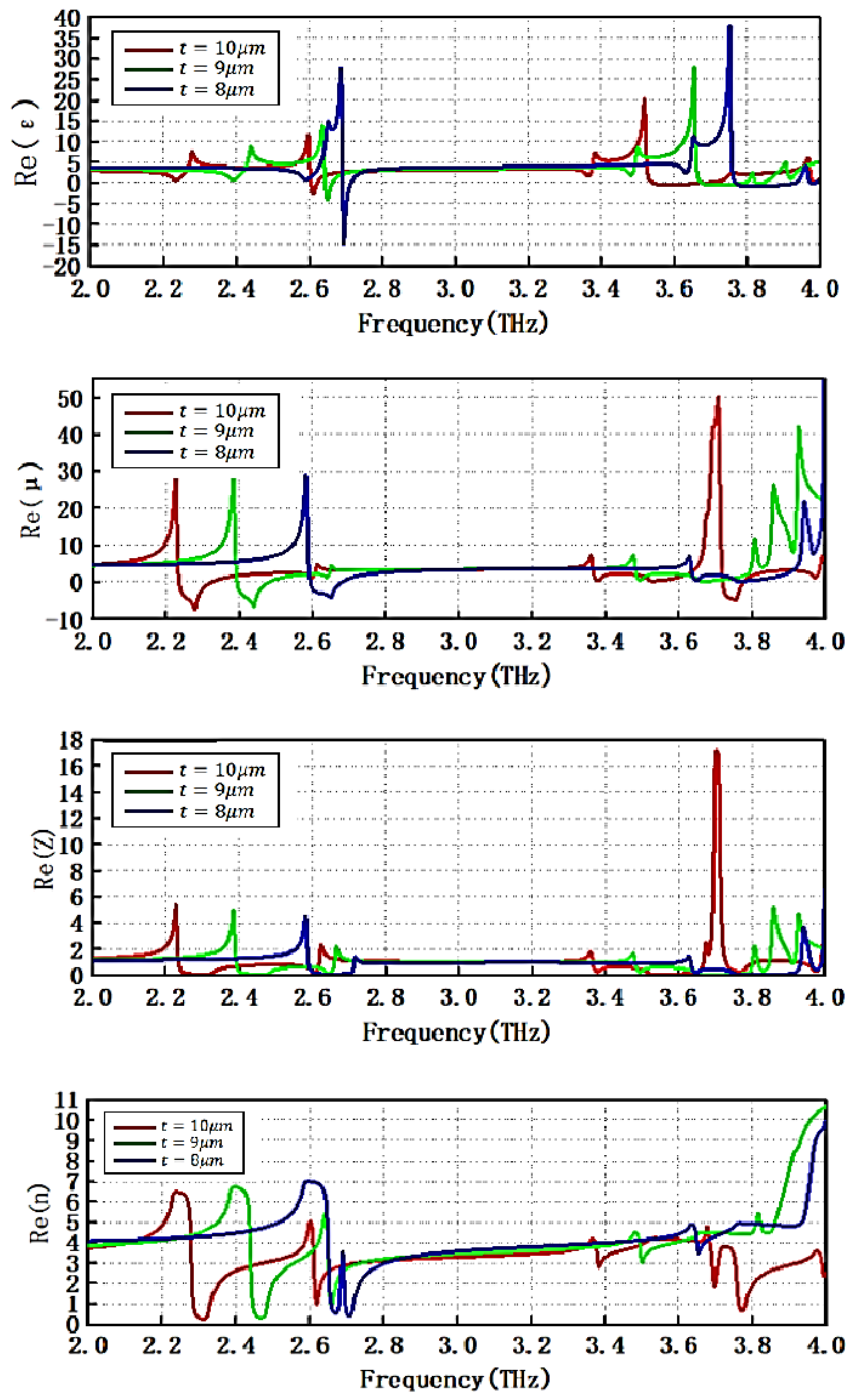
Fig. 11. Single square column height change (color online)
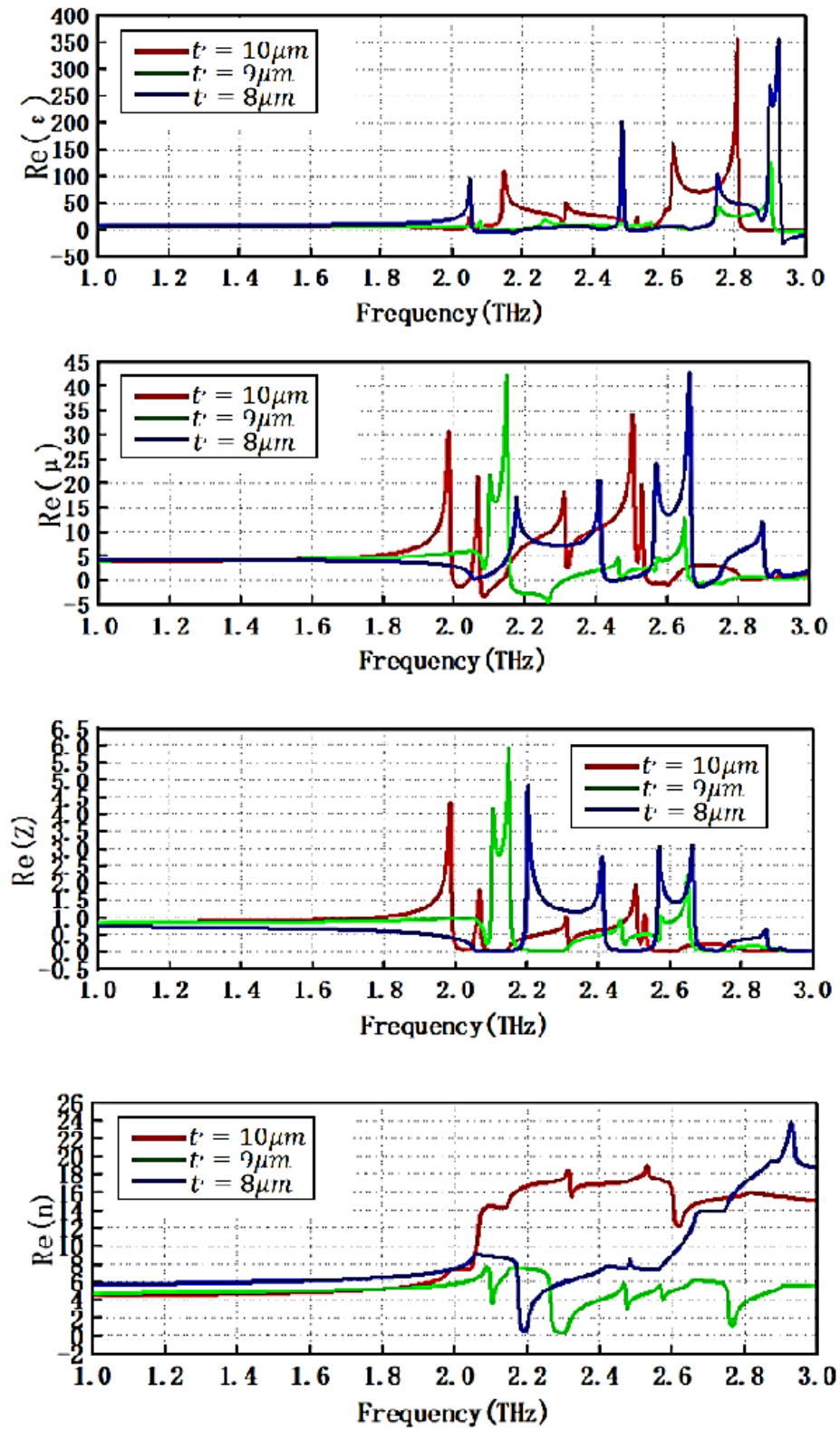
Fig. 12. Height variation of a square-pillar composite structure incident on a TE wave mode (color online)
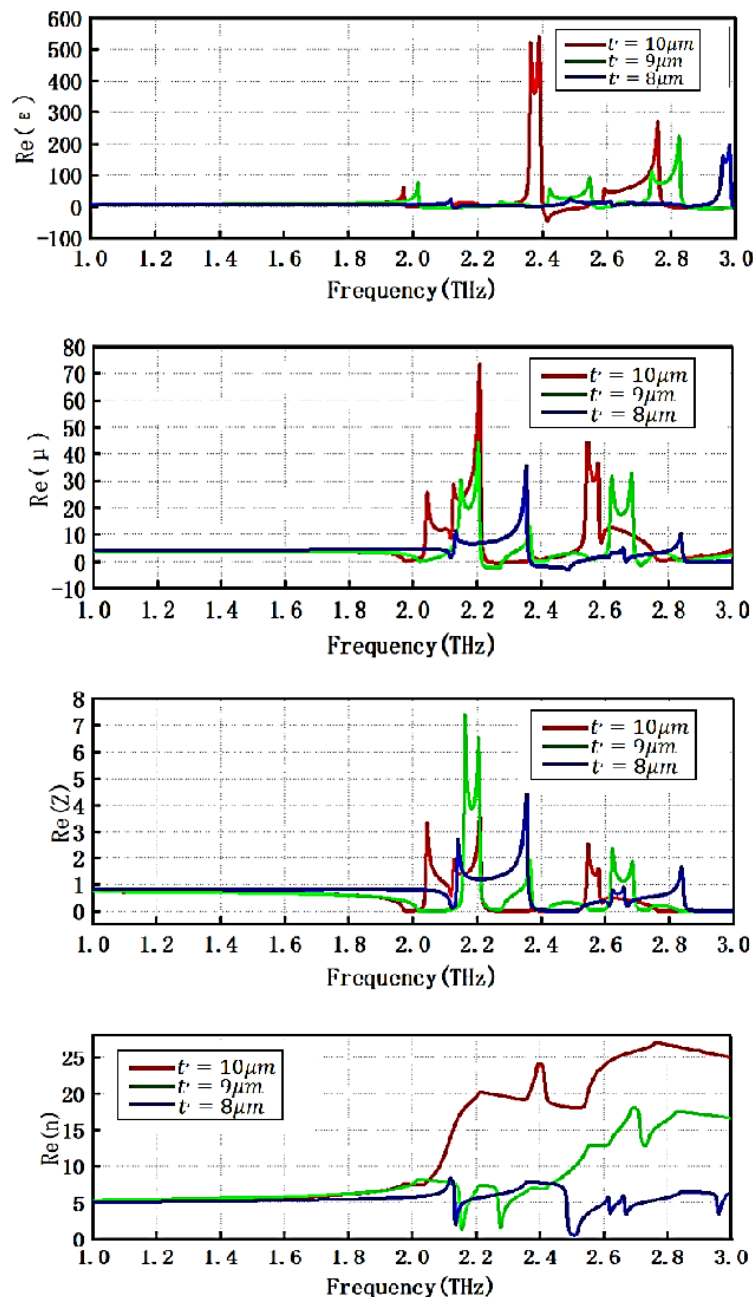
Fig. 13. Height variation of a square-pillar composite structure incident on a TM wave mode (color online)

As shown in Fig. 11, as the height of a single square column decreases, the resonance peak of the effective dielectric constant becomes larger, and the frequency corresponding to the peak becomes higher and higher. The peaks of effective permeability and effective impedance decrease with height, while the peaks correspond to higher and higher frequencies. The effective refractive index peak has an increasing trend, and as the peak becomes larger, the frequency corresponding to the peak becomes higher and higher. As shown in Fig. 12, when the TE mode is incident, when the height of the four square pillars varies, no obvious high-refractive-index broadband appears in the effective refractive index. As shown in Fig. 13, when the TM mode is incident, the change of the effective refractive

index is similar to that of the TE mode, and there is no obvious high refractive index broadband.

Next, we investigate the effect of changes in the structural period on the refractive index. When studying the effect of structural period changes on the refractive index, according to the optimization of the square-column composite structure, we choose the side lengths as a = 8.4 μm, b = 12.6 μm, c = 16.8 μm, d = 21 μm, and the height is t' = 10 μm. We choose a single square column to expand the side length by 1.2 times, that is, f = 16.8 μm. The height is t = 10 μm. The side lengths of a single square pillar structure base were changed to e = 42 μm, e = 45 μm and e = 48 μm, respectively. The side lengths of the four composite square pillar structures are e' = 42 μm, e' = 45

μm and e' = 48 μm, respectively. The corresponding effective parameters are shown in Figs. 14, 15 and 16. As shown in Fig. 14, with the increase of the side length of a single square column base, the effective dielectric constant is basically unchanged at the resonance peak at 2.6THz. The effective permeability and effective impedance are also basically unchanged. The effective refractive index peak does not change much. As shown in Fig. 15, when the TE mode is incident, when the combined structure of the four square columns changes periodically, the

frequency range corresponding to the high refractive index bandwidth does not change significantly, but the refractive index changes slightly. As shown in Fig. 16, when the TM mode is incident, the change of the effective refractive index is similar to that of the TE mode, and a resonance trough appears. To sum up, when the periodic side length of the substrate changes more and more, the square-column composite structure can form a high refractive index bandwidth, but the periodic variation basically has no effect on the broadband refractive index.
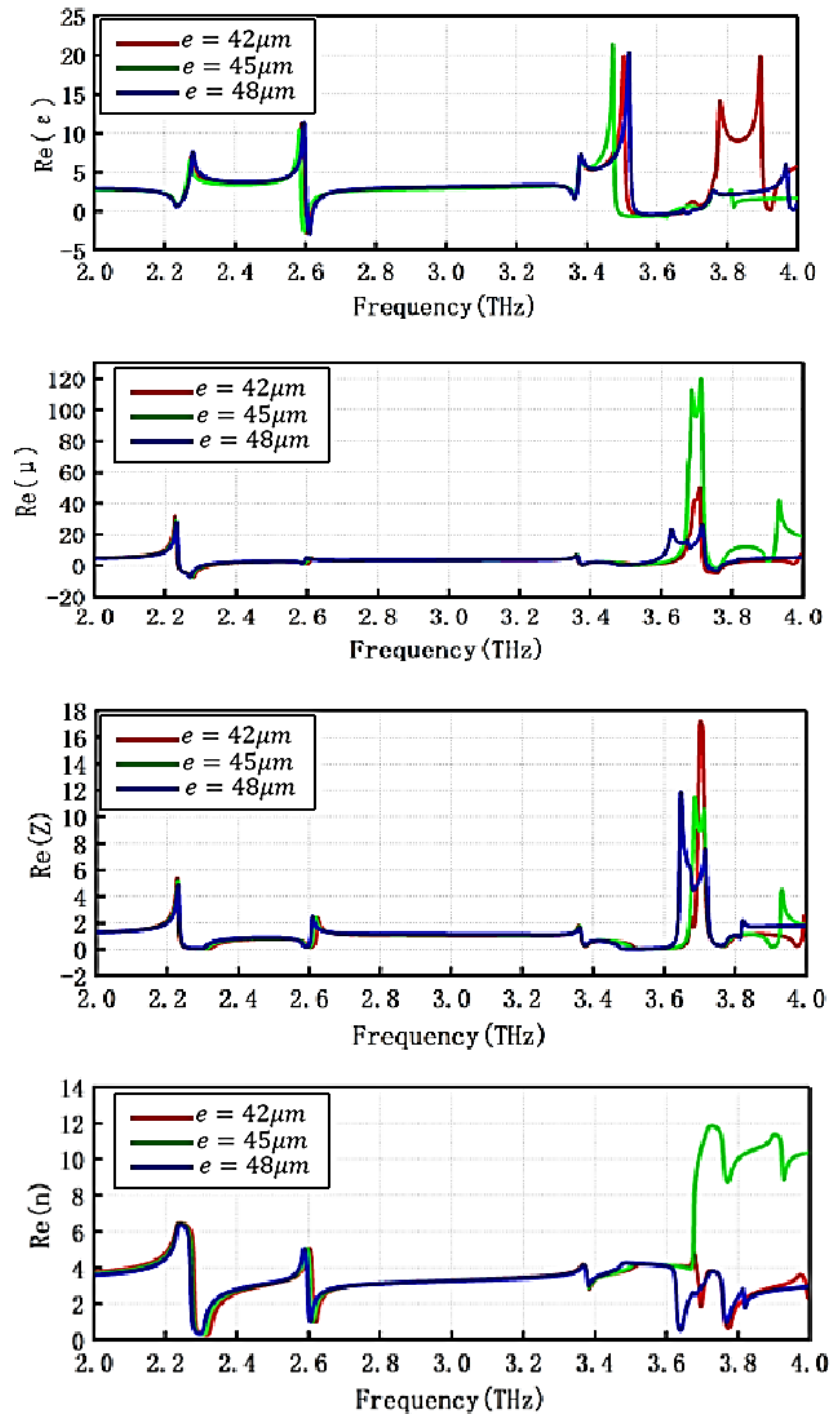
Fig. 14. Variation of the side length of the base of a single square column (color online)
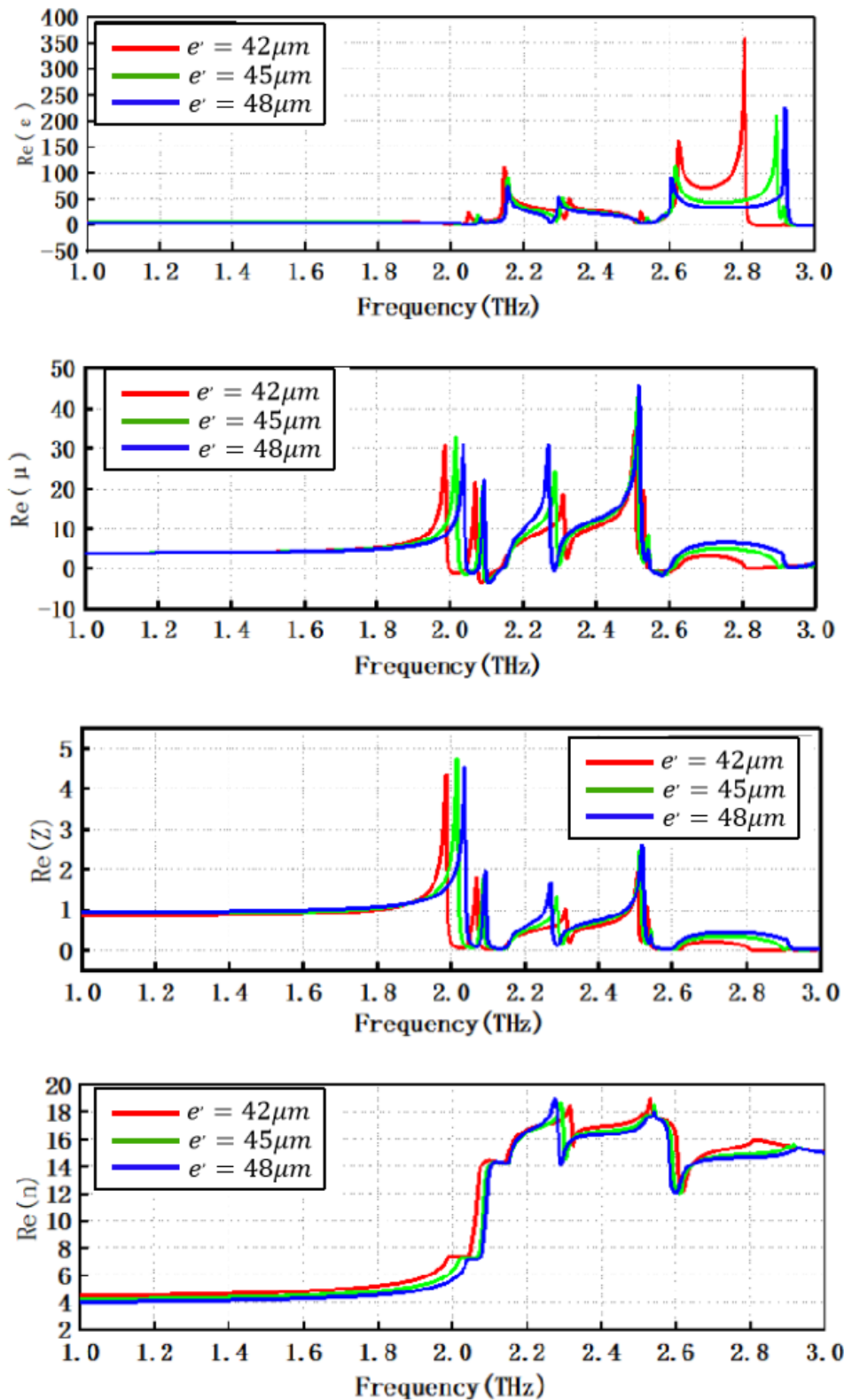
Fig. 15. Variation of the base side length of the composite square column structure when the TE mode is incident (color online)
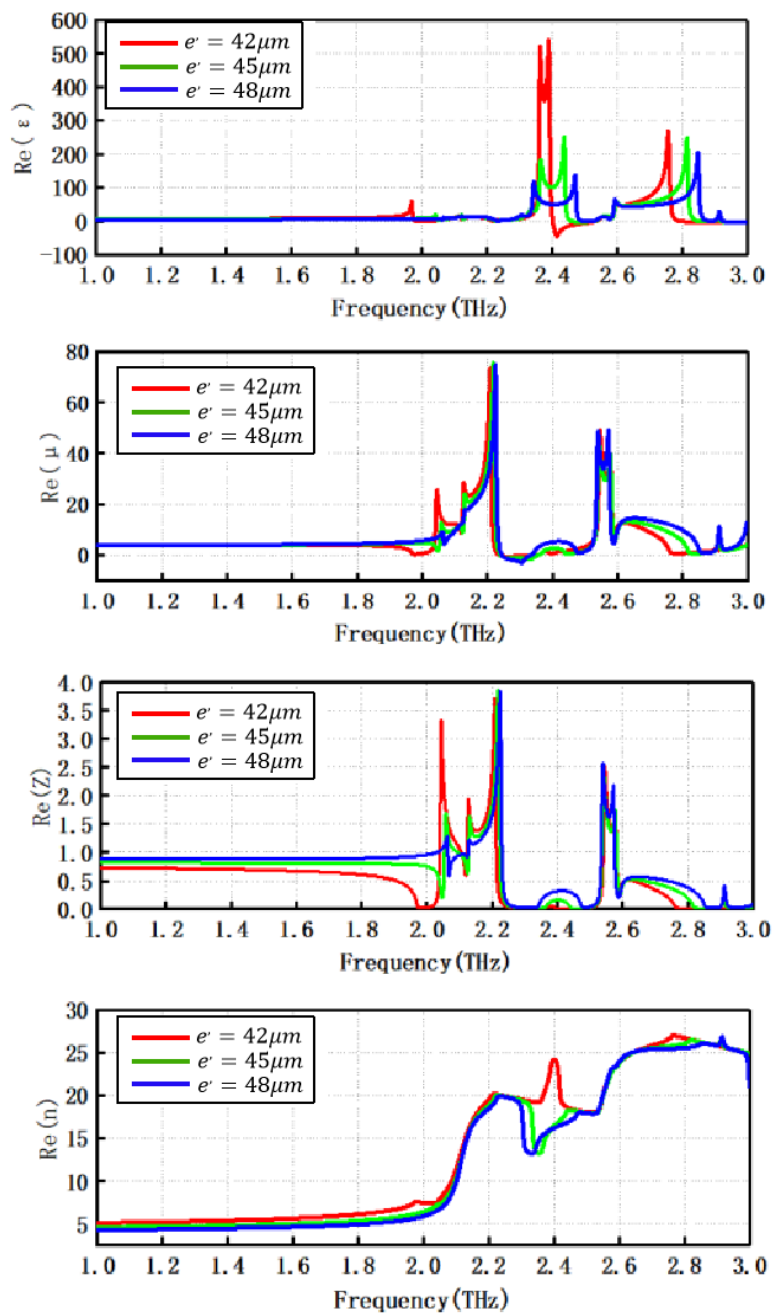
Fig. 16. Variation of the base side length of the composite square column structure when the TM mode is incident (color online)

Even though the presented work is fully based on numerical simulations of encoding metasurfaces, it is feasible to prepare such all dielectric encoding metasurfaces. The longer wavelength of THz waves requires an alternate fabrication process which is different to that previously described in the visible and infrared spectrum [48]. Detailed preparation process of all dielectric metasurfaces in terahertz range refers to Ref. [48]. The preparation processes include the base bonding, the conventional mask photolithography, and the Bosch deep reactive ion etching process [49-52].

4. Conclusions

Based on the high refractive index theory, a broadband high refractive metamaterial in the terahertz band is designed. The structure is composed of a single-layer composite structure of four square columns based on ultra-high dielectric constant materials, and exhibits square periodic arrangement characteristics. The effective refractive index calculated by the equivalent medium theory and the S-parameter inversion algorithm is above 15 in 2.48 THz ~ 2.97 THz, and the peak value is above 16, which is impossible for most materials in nature. We further study the effects of cell size, cell height, period,

etc. on the effective permittivity, effective permeability, effective impedance, effective refractive index, and frequency bandwidth and their changing trends.

References

[1] X. He, Carbon **82**, 229 (2015).

[2] X. He, X. Zhong, F. Lin, W. Shi, Opt. Mater. Express **6**, 331 (2016).

[3] Xiaoyong He, Feng Liu, Fangting Lin, Wangzhou Shi, Opt. Lett. **46**, 472 (2021).

[4] Xiaoyong He, Feng Liu, Fangting Lin, Wangzhou Shi, J. Phys. D: Appl. Phys. **54**, 235103 (2021).

[5] Jun Peng, Xiaoyong He, Chenyuyi Shi, Jin Leng, Fangting Lin, Feng Liu, Hao Zhang, Wangzhou Shi, Physica E, **124**, 114309 (2020).

[6] X. Jing, S. Jin, Y. Tian, P. Liang, Q. Dong, L. Wang, Optics & Laser Technology **48**, 160 (2013).

[7] X. Jing, Y. Xu, H. Gan, Y. He, Z. Hong, IEEE Access **7**, 144945 (2019).

[8] L. Jiang, B. Fang, Z. Yan, J. Fan, C. Qi, J. Liu, Y. He, C. Li, X. Jing, H. Gan, Z. Hong, Optics & Laser Technology, **123**, 105949 (2020).

[9] R. A. Shelby, D. R. Smith, S. Schultz, Science **292**(5514), 77 (2001).

[10] L. Jiang, Z. Yu, W. Zhao, Z. Yang, Y. Peng, Y. Zhou, X. Lin, S. Jin, Anal. Chem. **95**(2), 1721 (2023).

[11] H. Wang, L. Liu, C. Zhou, J. Xu, M. Zhang, S. Teng, Y. Cai, Nanophotonics **8**(2), 317 (2019).

[12] Ziyu Liu, Limei Qi, Feng Lan, Chuwen Lan, Jun Yang, Xiang Tao, Chin. Opt. Lett. **20**, 013602 (2022).

[13] Z. Yu, L. Jiang, R. Liu, W. Zhao, Z. Yang, J. Zhang, S. Jin, Chem. Eng. J. **426**, 131914 (2021).

[14] M. R. Akram, G. Ding, K. Chen, Y. Feng, W. Zhu, Advanced Materials **32**, 1907308 (2020).

[15] J. Zhang, X. Wei, I. D. Rukhlenko, H.-T. Chen, W. Zhu, ACS Photonics **7**(1), 265 (2020).

[16] Shunshuo Cai, Wanhan Hu, Yiman Liu, Juan Ning, Sixuan Feng, Chao Jin, Lingling Huang, Xin Li, Chin. Opt. Lett. **20**, 053601 (2022).

[17] Bo Fang, Zhiyu Cai, Yandong Peng, Chenxia Li, Zhi Hong, Xufeng Jing, Journal of Electromagnetic Waves and Applications **33**(11), 1375 (2019).

[18] B. Fang, B. Li, Y. Peng, C. Li, Z. Hong, X. Jing, Microw. Opt. Technol. Lett. **61**, 2385 (2019).

[19] Weimin Wang, Xufeng Jing, Jingyin Zhao, Yinyan Li, Ying Tian, Optica Applicata **47**(2), 183 (2017).

[20] L. Jiang, B. Fang, Z. Yan, C. Li, J. Fu, H. Gan, Z. Hong, X. Jing, Microwave and Optical Technology Letters **62**(6), 2405 (2020).

[21] R. Liu, C. Ji, J. Mock, J. Chin, T. Cui, D. Smith, Science **323**(5912), 366 (2009).

[22] X. Jing, W. Wang, R. Xia, J. Zhao, Y. Tian, Z. Hong, Appl. Opt. **55**(31), 8743 (2016).

[23] M. Choi, S. Lee, Y. Kim, S. Kang, J. Shin, M. Kwak, K. Kang, Y. Lee, N. Park, B. Min, Nature **470**, 369 (2011).

[24] M. O. Scully, Phys. Rev. Lett, **67**(14), 1855 (1991).

[25] J. B. Pendry, A. J. Holden, D. J. Robbins, W. J. Stewart, IEEE Transactions on Microwave Theory & Techniques **47**(11), 2075 (1999).

[26] D. Sievenpiper, E. Yablonovitch, J. Winn, S. Fan, P. Villeneuve, J. Joannopoulos, Phys. Rev. Lett. **80**(13), 2829 (1998).

[27] B. Wood, J. B. Pendry, J. Phys. Condens. Matter. **19**, 076208 (2007).

[28] J. Shin, J. T. Shen, S. Fan, Phys. Rev. Lett. **102**(9), 093903 (2009).

[29] Chunyan Jin, Wei Wu, Lei Cao, Bofeng Gao, Jiaxin Chen, Wei Cai, Mengxin Ren, Jingjun Xu, Chin. Opt. Lett. **20**, 113602 (2022).

[30] Pengfei Wang, Fengyan He, Jianjun Liu, Fangzhou Shu, Bin Fang, Tingting Lang, Xufeng Jing, Zhi Hong, Photon. Res. **10**, 2743 (2022).

[31] Yang Zhu, Binbin Lu, Zhiyuan Fan, Fuyong Yue, Xiaofei Zang, Alexei V. Balakin, Alexander P. Shkurinov, Yiming Zhu, Songlin Zhuang, Photon. Res. **10**, 1517 (2022).

[32] C. Gheorghiu, M. Cerchez, E. Aktan, R. Prasad, F. Yilmaz, N. Yilmaz, V. Leca, High Power Laser Science and Engineering **10**, 010000e3 (2022).

[33] G. Wang, J. Song, Y. Chen, S. Ren, P. Ma, W. Liu, P. Zhou, High Power Laser Science and Engineering **10**, 04000e22 (2022).

[34] T. Liu, M. Zhu, W. Du, J. Shi, J. Sun, Y. Chai, J. Shao, High Power Laser Science and Engineering **10**, 05000e30 (2022).

[35] J. Zhang, H. Zhang, W. Yang, K. Chen, X. Wei, Y. Feng, R. Jin, W. Zhu, Advanced Optical Materials **8**, 2000683 (2020).

[36] X. Bai, F. Kong, Y. Sun, F. Wang, J. Qian, X. Li, A. Cao, C. He, X. Liang, R. Jin, W. Zhu, Advanced Optical Materials **8**, 2000570 (2020).

[37] X. Jing, X. Gui, P. Zhou, Z. Hong, Journal of Lightwave Technology **36**(12), 2322 (2018).

[38] R. Xia, X. Jing, X. Gui, Y. Tian, Opt. Mater. Express **7**(3), 977 (2017).

[39] M. R. Akram, M. Q. Mehmood, X. Bai, R. Jin, M. Premaratne, W. Zhu, Advanced Optical Materials **7**, 1801628 (2019).

[40] Xiaoyong He, Wenhan Cao, Opt. Mater. Express **13**, 413 (2023).

[41] He Xiaoyong, Lin Fangting, Liu Feng, Shi Wangzhou, Nanophotonics **11**(21), 4705 (2022).

[42] J. Leng, J. Peng, A. Jin, D. Cao, D. Liu, X. He, F. Lin, F. Liu, Optics & Laser Technology **146**, 107570 (2022).

[43] L. Li, J. Wang, J. Wang, H. Du, H. Huang, J. Zhang, S. Qu, Z. Xu, Applied Physics Letters **106**(21), 212904 (2015).

[44] Haoliang Cheng, Bo Fang, Wenkang Huang, Ruisi Li, Changyu Shen, Lan Ke, Xufeng Jing, Chenxia Li, Zhi Hong, Optics and Laser Technology **156**, 108520 (2022).

[45] Xufeng Jing, Xiaoyan Tang, Ying Tian, Zhe Kong, Chenxia Li, Changyu Shen, Zhi Hong, Journal of Lightwave Technology **40**(1), 136 (2022).

[46] Xufeng Jing, Guihong Qin, Peng Zhang, Photonics Research **10**, 2876 (2022).

[47] Yu Liang, Yanyan Dong, Yongxing Jin, Lan Ke, Chenxia Li, Xufeng Jing, Infrared Physics and Technology **127**, 104441 (2022).

[48] Z. Ma, S. Hanham, P. Albella, B. Ng, H. Lu, Y. Gong, S. Maier, M. Hong, ACS Photonics **3**(6), 1010 (2016).

[49] C. Zhang, T. Xue, J. Zhang, Z. Li, L. Liu, J. Xie, J. Yao, G. Wang, X. Ye, W. Zhu, Biosensors and Bioelectronics **214**, 114493 (2022).

[50] C. Zhang, T. Xue, J. Zhang, L. Liu, J. Xie, G. Wang, J. Yao, W. Zhu, X. Ye, Nanophotonics **11**, 101 (2022).

[51] J. Zhang, N. Mu, L. Liu, J. Xie, H. Feng, J. Yao, T. Chen, W. Zhu, Biosensors and Bioelectronics **185**, 113241 (2021).

[52] R. Liu, L. Jiang, Z. Yu, X. Jing, X. Liang, D. Wang, B. Yang, C. Lu, W. Zhou, S. Jin, Sensor. Actuat. B-Chem. **333**, 129581 (2021).

_____

[*]Corresponding author: 28361682@qq.com